

## Research Article

## Hydraulic Valve for Miniature Surgical Robot Applications

D.R. Berg<sup>a\*</sup> and P.Y. Li<sup>b</sup><sup>a</sup>*Engineering and Technology Department, University of Wisconsin-Stout, Menomonie, WI, USA;*<sup>b</sup>*Department of Mechanical Engineering, University of Minnesota, Minneapolis, MN, USA**(v1.0 released July 2017)*

This paper describes the design and testing of a novel hydraulic control valve for use in the minimally invasive surgical robotic manipulator. The use of hydraulics for surgical robotics opens new possibilities for miniaturization and robustness. However, to enable this, there exists a need for hydraulic components which bridge the size gap between traditional fluidics and microfluidics. This paper provides motivation for the development of a miniature hydraulic valve designed specifically to enable a serpentine style hydraulic surgical manipulator. Included are a description of the various considerations relevant to the valve and its specific application, such as the method of manipulation for the valve, as well as a theoretical valve design and a mathematical description of the operating principles. Two possible methods of valve activation, piezoelectric and electromagnetic, are discussed along with two physical realizations of the valve design are presented which demonstrate the theoretical design. Finally, the results of experimental testing performed on valve prototypes is described to evaluate the design options and help inform the selection of the final configuration.

**Keywords:** hydraulic valve; surgical robotics; minimally invasive surgery; surgical tools; NOTES

## 1. Motivation and Related Work

The use of robotics in surgery is becoming increasingly necessary with the advent of new minimally invasive surgical techniques such as single port access (SPA) surgery, a single incision procedure during which access to the abdominal cavity is typically gained through the navel, and natural orifice transluminal endoscopic surgery (NOTES), an experimental technique that involves performing traditional surgical procedures with a flexible endoscope through one of the body's natural orifices [1]. One approach to the development of surgical robots is fluid power. For example, work is currently in progress exploring the use of fluid power at the meso-scale (mm to cm) for use in prosthetics [2]. The next logical step is to explore the use of fluid power at the micro-scale ( $\mu\text{m}$  to mm) for which the research is ongoing in the field known as microfluidics [3, 4]. However, as pointed out by Love et al., there exists a gap between conventional fluidics and microfluidics that includes the type of high pressure-low flow rate fluid power components that would be necessary for the application of hydraulic power to the field of surgical robotics [2]. Therefore, it is necessary to conceptualize the methods by which these sorts of fluid power components might be realized to satisfy a growing need as designers of surgical robots look to fluid power [5–7]. This paper describes the design of a flow control valve targeted at miniature surgical applications and specifically a natural orifice surgical robot described in Berg, 2013 [5] (herein referred to as ‘this application’).

---

\*Corresponding author. Email: bergdev@uwstout.edu

The ability to control the flow of the fluid is essential to any hydraulic system. Typically this is achieved through the use of valves which can control whether the flow is ON or OFF and possibly the rate at which the fluid is flowing. The method by which flow is stopped can include rotational motion such as in a rotary valve, linear motion such as in spool or poppet valves, or with a flapper valve that acts parallel to the flow direction. Additionally, proportional control can be achieved through varying the size of the valve opening or by control of an ON/OFF valve. Either method carries advantages and disadvantages. A proportional valve may provide more straight forward control methods; however, it introduces additional difficulties such as power consumption which can be particularly troublesome for small scale applications. Alternatively, an ON/OFF valve may have a simpler design but considerations must be made for inertial and transitional losses. Another possible solution is the use of digital hydraulics which enables a near analog output using digital or ON/OFF components [8]. For all methods, precise flow control is an integral component of a successful hydraulic system.

There has been a significant amount of research committed to the design and evaluation of flow control valves. However, the area particularly relevant for surgical applications is valve miniaturization due to the limited space availability within the surgical tool. The field of fluid power at the micro-scale is commonly referred to as microfluidics, a field with origins beginning in the 1990s and has quickly expanded to suit a variety of potential applications [4]. Much of the research in microfluidic valves makes use of any one of a short list of enabling technologies including electrostatic, magnetic, piezoelectric, thermal, chemical, or pneumatic methods [9–14]. Of these options, possible valve operation methods such as piezoelectric or electrostatic can provide interesting solutions to the problem of flow control and have been explored extensively for control of pneumatic systems [15, 16]. For many miniature surgical applications, microfluidic devices do not provide sufficient flow rates to enable devices that are simultaneously small and fast. New devices found in the literature will require components that bridge the gap between traditional and microfluidics.

A suitable valve for miniature surgical applications which meets the requirements in terms of controllability and within a size limit of six millimeters outer diameter (quantified in [5]) was not found to be available commercially. However, there are several approaches being pursued academically to bridge the gap between traditional and microfluidics. Two methods presented in the literature include the use of magnetics for valve actuation [17, 18]. Fu et al. present a solution designed to use 3 mm diameter iron balls to facilitate closure of the valve orifice [17]. The position of the ball is driven by a coil with a length of 10 mm and a diameter of 8 mm. The valve was demonstrated to operate with supply pressures of 50 kPa to 200 kPa and could operate in proportional mode up to 112.5 kPa before the ball was pulled into the valve seat. This design is promising but has too large of a footprint and operates at too low of pressures for use in this application. Another solution presented by Pernod et al. has a similar pressure capacity and is operated by a 1 mm long by 3 mm diameter permanent magnet combined with a 500 winding coil to manipulate the valve membrane [18]. This valve has a smaller footprint than the design presented by Fu et al. but does not yet meet the requirements for this application in terms of size and controllability. Finally, Peirs et al. investigated the use of both electromagnetic and piezoelectric methods for valve manipulation [19]. In that study it was found that either approach provided significant challenges for producing the desired performance safely and consistently. In particular they encountered challenges with integrating the valves into their design under similar size constraints to the present application. Therefore, given the lack of available solutions either commercially or academically, the design of a new valve to fit this application and meet the necessary design considerations was undertaken.

## 2. Control Valve Design

In order to achieve precise manipulation, it is necessary to obtain a control valve that will provide a controllable actuator pressure while occupying as little space as possible within the device. A review of the available commercial valves and common microfluidic valve solutions was conducted and no existing valve design was found suitable for the present application due to the limitations of high supply pressure, proportional control, and method of activation. Therefore, development of a novel control valve with a diameter of 6 mm, capable of manipulating high pressure flows, which could be on the order of 0.7 to 7 MPa for hydraulics, on a small scale was performed.

For this application, the outlet of the valve will be connected to an artificial muscle actuator [20]. To provide useful manipulation, it is the feed pressure,  $P_a$ , to the actuator that must be regulated by the valve such that the contractile force produced by the actuator, which is proportional to  $P_a$ , can be manipulated. Each actuator provides one directional contraction only and thus an arrangement of three actuators at a minimum operated differentially and antagonistically such that the manipulator can operate in three-dimensional space using three hydraulic actuators. For each of the actuators, a simple hydraulic circuit such as is shown in Fig. 1 can be used. This circuit consists of an upstream, high-pressure supply,  $P_s$ , and a fixed orifice flow restriction,  $R_1$ , as well as a downstream variable orifice flow restriction,  $R_2(t)$ , and a return to atmosphere,  $P_{atm}$ . Between the two flow restrictions is the feed point for the actuator,  $P_a(t)$ . By adjusting the downstream restriction relative to the fixed, upstream restriction it would then be possible to manipulate the pressure at the actuator feed point as a pressure divider. For this purpose, a flapper-style valve can be used as a variable orifice [21]. With appropriately sized orifices, the flapper would then act as the input for manipulating the downstream orifice within its available stroke range.

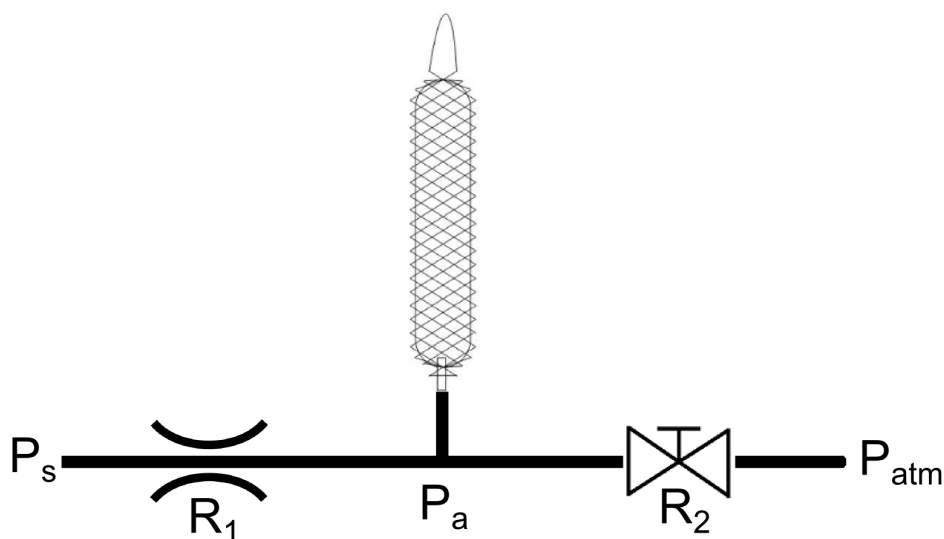


Figure 1.: Hydraulic circuit concept for control of a single actuator.

As each manipulator segment would require three actuators, the hydraulic circuit could be modified to the form shown in Fig. 2, which shows three sets of upstream orifices, three actuator feed points, and a single central flapper that is used to regulate the three actuators in a differential/antagonistic fashion as required. As such, when the flapper moves nearer to one of the downstream exit orifices (increasing the pressure at the associated actuator feed point), it is moving away from the other two exit orifices at the same time (decreasing the pressure at the associated actuator feed points).

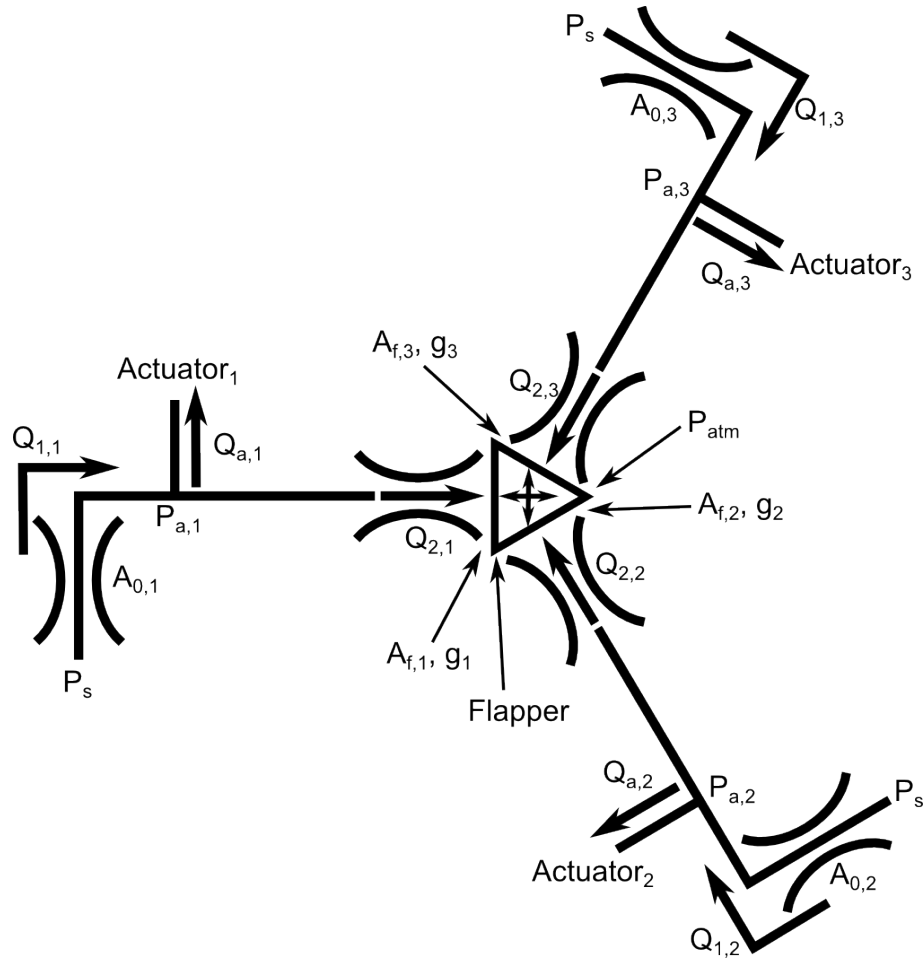


Figure 2.: Three actuator hydraulic circuit concept for the flapper style valve design.

This style of valve has the advantages of low complexity and insensitivity to contaminants in the fluid [21]. Further, the manipulation of the valve can be intuitively mapped to the output of the manipulator since each have three inputs and are operated differentially/antagonistically. One of the basic principles of a flapper style valve is that there is a constant leakage flow. Thus the supply must be capable of accommodating the leakage. This presents little concern as the flow rate required to inflate artificial muscle actuators of this scale is significantly smaller than the available flow rate of the supply, five liters per hour based on actuator fill time (assuming 689 kPa supply pressure, 0.5 seconds fill time for a single actuator) for a design scale actuator versus 55 liters per hour based on available flow rate for common endoscopic irrigation pumps [21, 22]. Further, the capabilities of existing irrigation pumps do not constrain the design as the supply pump could be modified to meet the necessary requirements.

### 3. Analytical Description of Flapper Based Valve Design

The valve design is modeled as a flapper style valve and thus the flow through each upstream orifice ( $Q_{1,i}$ ) and each downstream valve orifice ( $Q_{2,i}$ ), shown in Fig. 2, is calculated in Eqs. 1 and 2.

$$Q_{1,i}(t) = A_0 C_{d0} \left[ \frac{2}{\rho} (P_s - P_{a,i}(t)) \right]^{\frac{1}{2}} \quad (1)$$

$$Q_{2,i}(t) = A_{f,i}(t)C_{df} \left[ \frac{2}{\rho}P_{a,i}(t) \right]^{\frac{1}{2}} = \pi D_N g_i(t)C_{df} \left[ \frac{2}{\rho}P_{a,i}(t) \right]^{\frac{1}{2}} \quad (2)$$

where  $P_s$  is the supply pressure and  $P_{a,i}$  is the pressure at each actuator feed point. Here it is shown that the upstream flow rate is consistent with the standard orifice equation, where  $A_0$  and  $C_{d0}$  are the area and discharge coefficient of the upstream orifice, respectively, while the downstream flow exiting the downstream orifice is restricted by the flapper. In this case the curtain area ( $A_{f,i}(t)$ ) rather than the orifice area is used in the flow rate calculation. The curtain area is  $\pi D_N g_i(t)$ , where  $D_N$  is the nozzle diameter and  $g_i(t)$  is the gap between the orifice and the flapper. Further, the discharge coefficient for the flapper orifice ( $C_{df}$ ) is typically on the order of  $0.8 \cdot C_{d0}$  [21]. In both of the previous equations,  $\rho$  represents the density of the fluid used. The gap,  $g_i(t)$ , acts as the input variable for control of the valve and varies based on the spatial position of the flapper. If the three-dimensional position of the flapper is described in Cartesian coordinates where the XY-plane describes planar motion of the flapper and the Z-axis describes out-of-plane motion, then the change in the size of the gap,  $g_i(t)$ , can be found as

$$\begin{bmatrix} \Delta g_1(t) \\ \Delta g_2(t) \\ \Delta g_3(t) \end{bmatrix} = \begin{bmatrix} 1 & 0 & -\sin \beta \\ -\sin 30^\circ & \cos 30^\circ & -\sin \beta \\ -\sin 30^\circ & -\cos 30^\circ & -\sin \beta \end{bmatrix} \begin{bmatrix} \Delta x(t) \\ \Delta y(t) \\ \Delta z(t) \end{bmatrix} \quad (3)$$

assuming that the gap,  $g_1$ , is aligned with the X-axis and  $\beta$  is the taper angle of the flapper as discussed further in Section 5. Equation 3 assumes that the downstream orifices are equally spaced around the circumference of the valve and that a positive change in  $g_i(t)$  corresponds to closure of the gap.

Additionally, the flow rate to or from the actuator must satisfy the difference between the upstream and downstream flow rates for each actuator as in Eq. 4.

$$Q_{a,i}(t) = Q_{1,i}(t) - Q_{2,i}(t) \quad (4)$$

Since  $Q_{a,i}(t)$  is equal to the rate of change of actuator volume,  $\dot{V}_i(t)$ , under the incompressibility assumption, actuator flow rate,  $Q_{a,i}(t)$ , is assumed to be a known input to this valve system.

It is convenient to establish the working range of the control pressure by examining the blocked-load condition,  $Q_{a,i}(t) = 0$ . In this steady-state condition when actuator volume is constant, the upstream and downstream flow rates become equal and the equations simplify to

$$\frac{P_{a,i}}{P_s} = \left[ 1 + \left( \frac{C_{df}A_{f,i}(t)}{C_{d0}A_0} \right)^2 \right]^{-1} \quad (5)$$

This relationship is shown in Fig. 3 [21]. This plot shows that there is a large region of approximately linear response between 0.4 and 1.6 for the orifice ratio. Further, it can be seen that the pressure response flattens out at an orifice ratio of approximately 3.0, meaning that this is a reasonable upper limit placed on the size of the flapper valve exit area relative to the upstream flow restriction.

#### 4. Valve Actuation

Under the conditions described in the previous section, it is necessary to consider the options available to provide operation of the valve. The two most promising solutions are piezoelectric and electromagnetic [15, 16]. The mechanism used for valve actuation must be able to fit within the constraints of the device and the available space within the valve, manipulate the three downstream orifices either with one component or three single-acting components, and provide

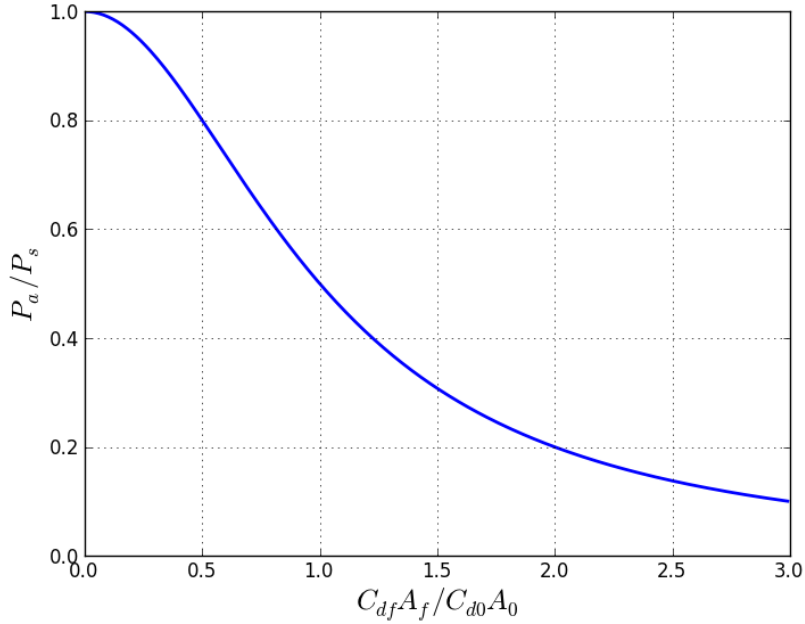


Figure 3.: Plot of pressure ratio versus orifice ratio for a flapper valve.

analog manipulation over the range of motion specified in Section 3. Some work exploring the use of PZ actuators for valve control has been presented in the literature where it was suggested that a PZ stack can be used effectively for this application but care must be taken to limit the effects of moisture [19]. Further, while large forces are possible with PZ actuators, large displacements are difficult to produce, typically in the range of 0.1% strain as a maximum [23].

Electromagnetic actuation is another option for manipulation of the valve discussed in Section 2. The use of this type of actuation has the disadvantage of not being MRI compatible but has the advantages of being low complexity, inexpensive, and able to operate in an aqueous environment. The basic realization of an electromagnetic actuator is such that a magnetic field is generated by wound coils of small diameter magnet wire. An example of a coil produced using 44 AWG (American Wire Gauge) wire which has a diameter of 0.05 mm is shown in Fig. 4. The key design parameter for the driving coil is the wire diameter which is available commercially in a variety of discrete sizes. The resistance of the wire is then directly a function of the wire diameter and length necessary to produce the coil. Further, the current applied to the wire is variable such that the coil produces the desired electromagnetic force to manipulate the valve. The driving coil has to be capable of closing the gap between the coil and the flapper against the force of the saline exiting the orifice. The force that the solenoid is capable of producing can be calculated by first finding the magnetic flux density,  $B$ , from Ampere's Law [24] as

$$B = \frac{NI\mu}{g} \quad (6)$$

where  $I$  is the coil current,  $N$  is the number of coil turns,  $g$  is the gap between the solenoid and the flapper, and  $\mu$  is magnetic permeability of the core material. Force generated can then be expressed as

$$F = \frac{B^2 A}{2\mu} = \frac{(NI)^2 \mu A}{2g^2} \quad (7)$$

where  $A$  is the cross sectional area of the solenoid. By rearranging Eq. 7 the current requirement

for closure of an electromagnetic relay can be shown as

$$I = \sqrt{\frac{2g^2 F}{N^2 \mu A_N}} = \frac{g}{N} \sqrt{\frac{2F}{\mu A}}. \quad (8)$$

It is apparent that the closing force,  $F \propto I^2 N^2$ . Further, it is necessary to consider that the possible number of coil turns,  $N \propto \frac{1}{D_w^2}$  based on circle packing density [25] and  $I \propto D_w^2$  for a given force requirement based on wire resistance being inversely proportional to cross-sectional area, where  $D_w$  is the wire diameter. Putting these relationships together demonstrates that the closing force capacity of a given coil is independent of wire diameter. Another consideration is the power consumed by the coil during operation. Knowing that the power carried by the wire is related to current and resistance as  $P = I^2 R$ , it is seen that  $P \propto D_w^2$  as well since wire resistance,  $R \propto \frac{1}{D_w^2}$ . This implies that for larger wire diameter, more power is introduced to the system and thus more heat has to be dissipated from the driving coil in order to prevent a short by melting the wire insulation. This suggests that the smallest possible wire would be the most ideal for the coil in terms of heat dissipation from the system. One additional benefit to selecting the smallest possible diameter for the coil wire is that as the diameter decreases, the achievable packing density for a given available space increases [25]. By optimizing the packing density, it is possible to achieve the necessary force capacity from the solenoid for a smaller outer diameter. For problems of this sort, it is found that the packing density converges towards a volumetric efficiency of 90.69% as the wire diameter decreases [26]. For this application, greater than 90% efficiency is achieved for diameters smaller than 0.21 mm, based on the analysis of Peikert et al., 1992 [25]. Therefore, any wire diameter smaller than this limit provides reasonable packing density. Given this analysis and the available sizes of magnet wire, wire with a diameter of 0.05 mm was selected for prototyping and testing purposes.



Figure 4.: Photograph of a 44 gauge wire coil used to test heat dissipation.

Revisiting Eq. 8, it is possible to apply the design constraints set forth in Section 3

$$\frac{C_{df} A_f}{C_{d0} A_0} = 3 \quad (9)$$

and  $C_{df} = 0.8 \cdot C_{d0}$  together with the equation for the flapper gap

$$g = \frac{A_f}{\pi D_N} = \frac{3.75 A_0}{\pi D_N}. \quad (10)$$

If the force requirement for the flapper is equal to the pressure drop across the valve multiplied by the nozzle area,  $A_N$ , then Eq. 8 becomes

$$I = \frac{g}{N} \sqrt{\frac{2P_a}{\mu}}. \quad (11)$$

Finally, the number of coils of wire,  $N$ , that can fit within can be approximated using the optimal packing density of 90.69% and the available area,  $L_c \cdot D_c/2$ , where  $L_c$  and  $D_c$  are the length and effective diameter of the coil, as

$$N = \frac{L_c \cdot D_c \cdot 0.9069}{\frac{\pi}{4} D_w^2}. \quad (12)$$

Putting it all together,

$$I = \frac{3.75 A_0}{\pi D_N} \cdot \frac{\frac{\pi}{4} D_w^2}{L_c \cdot D_c \cdot 0.9069} \cdot \sqrt{\frac{2P_a}{\mu}}. \quad (13)$$

Substituting in the appropriate values for this design and assuming 242 turns of wire are used to form the coil around a steel core, determined experimentally, it is found that the necessary driving current is 41.0 mA. Therefore, based on the wire diameter previously selected, it is calculated that the power being dissipated into the system is on the order of 7.8 mW where the resistance of the wire is calculated using the resistivity of standard copper.

Since the energy entering the system through the coil is primarily dissipated through heat, it is necessary to determine how much of that heat can be delivered into the fluid that is flowing past the coil. To evaluate this, it is necessary to develop an understanding of the capacity of the fluid to remove heat from the coil as it passes through the valve. The heat transfer coefficient for this flow is calculated as

$$h = \frac{k_w}{D_H} Nu \quad (14)$$

where  $k_w$  is the thermal conductivity of the fluid,  $D_H$  is the hydraulic diameter of the flow path, and  $Nu$  is the Nusselt number. As the flow within the valve is likely to be turbulent based upon the flow rate of the fluid and the diameter of the orifices, the Dittus-Boelter correlation [27] was used to calculate  $Nu$  as

$$Nu = 0.023 Re^{0.8} Pr^n \quad (15)$$

where  $Re$  is the Reynolds number (10,298) calculated on the basis of the hydraulic diameter,  $Pr$  is the Prandtl number (13) estimated for 0.9% water salinity [28], and  $n$  is equal to 0.4 since the coil temperature is greater than the fluid temperature (heating condition) [29]. Finally, the heat flow in watts is calculated as shown in Eq. 16 where  $A$  is the surface area of the fluid interaction and  $\Delta T$  is the temperature difference between the coil and the bulk fluid.

$$Q = hA\Delta T = \frac{k_w}{D_H} NuA\Delta T \quad (16)$$

Substituting in the design parameters for this valve [5] and the properties of saline ( $k_w = 578.8 \frac{mW}{m \cdot K}$  [30, 31]) it is found that the available heat flow into the bulk fluid is on the order of 166 mW per unit kelvin of temperature difference. Thus as the temperature difference increases, the heat flow into the fluid increases as well. Since the total capacity for heat flow into the fluid is significantly greater than the maximum power entering the coil, the coil temperature should stabilize below the melt temperature of the wire insulation even when operating at maximum current.

## 5. Description of Valve Realizations

Two possible realizations of this valve design were explored. The first consists of three flapper nozzle valves [21] controlled by one single tetrahedral valve plug that plays the role of the flapper for each of the orifices (see Fig. 5). A second realization (Fig. 6) of the flapper style valve design was also developed, which differs from the first design in that the supply enters the valve at the center and exits radially as shown in Fig. 9, opposite the orientation of the first design. With this design the orifices are located on the outer diameter of the valve body and are opened or closed using a ring which is manipulated radially.

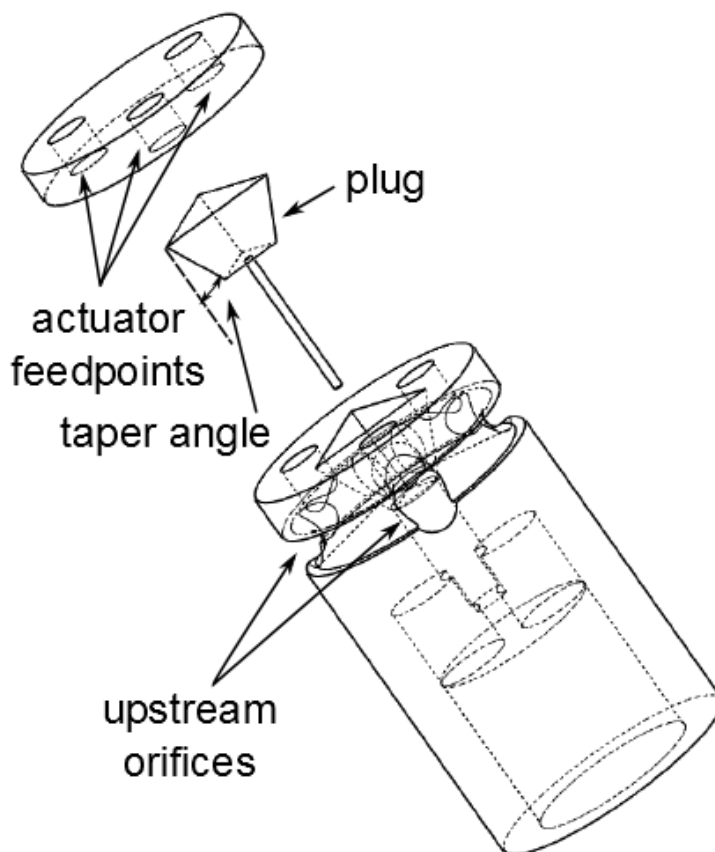


Figure 5.: Exploded view of the plug-based valve model showing the valve body and internal components.

This valve design is normally open such that the majority of the flow bypasses the actuator and dumps to the return line. When the manipulated part (plug or ring) is activated in a particular in-plane direction, the orifices are activated differentially: the orifice(s) that the plug gets closer to become more restrictive, and the corresponding actuator pressures increase; the

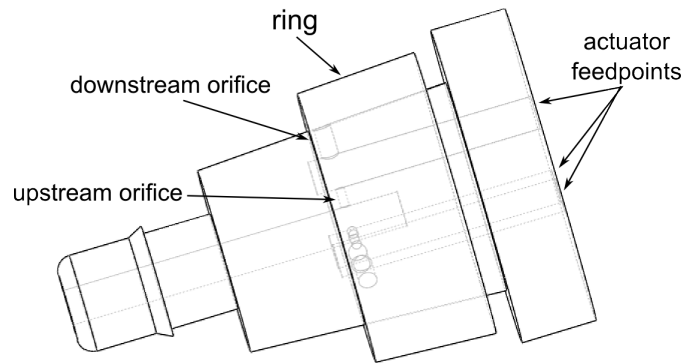


Figure 6.: Model of ring based flapper valve design.

orifice(s) that the manipulated part gets further away from becomes less restrictive, and the corresponding actuator pressures decrease. This in turn produces a directional actuation of the manipulator to bend in the direction where the orifices become more restrictive. Out of plane movement of the manipulated part pressurizes or de-pressurizes the actuators simultaneously. This has the effect of increasing or decreasing the manipulator stiffness and also provides the ability to independently manipulate the pressure at the three actuator feed points. These orifices are sized based upon the necessary flow rate and the valve characteristics described by Eq. 5 [5].

### 5.1 Plug-Based Valve Design

The plug-based valve consists of a single supply pressure input which feeds three upstream (fixed) orifices (Fig. 5) [32]. The central plug is manipulated electromagnetically (Fig. 7) by three independent control signals. The tetrahedral shaped valve plug can move both in plane and out of plane and can be manipulated to block each downstream (variable) orifice individually, in pairs of two, or all three depending on how the control signals are applied. When an orifice is blocked, pressure increases at the feed point for the corresponding actuator. Conversely, when the orifice is unblocked, flow passes to the return line and pressure at the actuator feed point decreases. Figure 8 shows one third of the flow path when the variable orifice is open (top) and when the orifice is blocked (bottom). In the open position, the majority of the flow passes through the valve following the least resistance path and exits to the return line. When the variable orifice is blocked, the path to the return line has a high flow resistance and thus more of the fluid flow feeds into the actuator.

### 5.2 Ring-Based Valve Design

A second realization of the flapper style valve design was also developed and prototyped (see Fig. 6) [33]. For this version of the valve, the operation principles are the same as for the previous version. The primary difference for this design is that the supply enters the valve at the center and exits radially as shown in Fig. 9, opposite the orientation of the other valve version. The flapper nozzles are located on the outer diameter of the main valve body. These orifices are opened or closed differentially using a ring placed over the orifices and manipulated radially (Fig. 6). Further, both the valve body and the ring are tapered to allow for stiffness control of the three actuators together (see example in Fig. 10). With a greater taper angle, the travel distance along the long axis of the valve that is necessary for the ring to open or close the downstream orifice is reduced. This in turn results in a ring that is smaller and thus easier to manipulate. However, the smaller ring with a higher taper angle becomes more difficult to manufacture and is more sensitive thus requiring more precise manipulation.

One of the primary advantages of the ring-based valve design over the plug-based design is

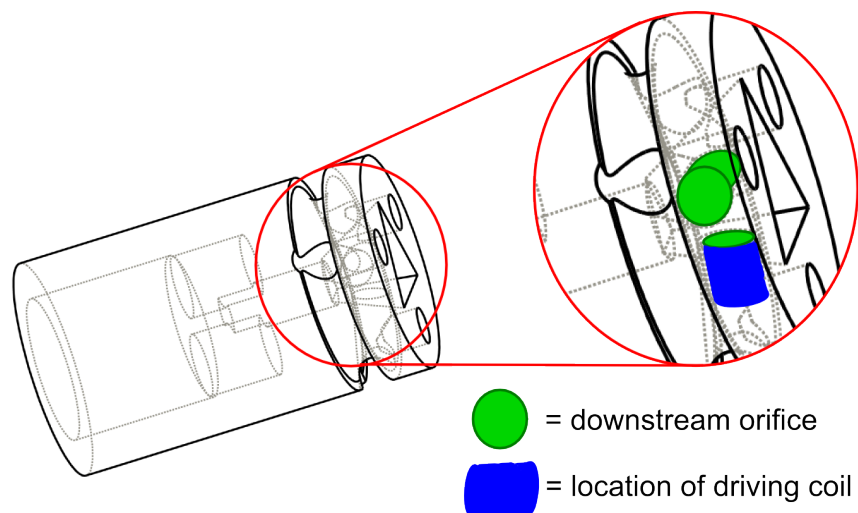


Figure 7.: Enlarged view of plug-based valve showing downstream orifices and location of a single driving coil.

that this design is more easily produced using conventional machining techniques. For example, it is possible to fabricate this design using a standard lathe.

### 5.3 Valve Connection for Supply and Return Lines

The design of each valve geometry is such that both the high-pressure supply and the low-pressure return lines can connect to the valve body in a direction parallel to the longitudinal axis of the valve. This method of connection keeps the overall size requirements of the valve in the radial direction as small as possible. One realization of this method of connection would employ a hydraulic line with the cross-section shown in Fig. 11, where the black areas represent the tubing material and the inner white areas represent the multiple lumens of the tubing. This tubing is then connected to the base of the valve body such that the outer two lumens pass over the lower portion of the valve body and are sealed to the valve at the distal outer diameter as shown in Figs. 12. The inner lumen passes inside the inner diameter of the base of the valve body and is sealed to this inner wall or the barbed fitting. The hydraulic supply and return then behave as shown in Figs. 8 and 9. The use of this style of tubing permits the option of supplying the valve by running the tubing down the length of the endoscope working channel and connecting to an external pump located in the surgical suite. However, when more than one valve is placed in series within the working channel such as would be necessary with a multi-segment manipulator, providing space for the tubing from the distal valve to bypass the proximal valve may prove challenging.

Another option is to utilize the existing irrigation and suction channels common to most current endoscopes. These channels exist to facilitate surgical procedures by flushing the surgical site of debris and removing fluids from the site, respectively. Making use of these existing fluid channels would reduce the number of lines running the length of the endoscope and eliminate the need for a secondary external fluid pump as existing endoscopic irrigation pumps are typically capable of meeting the design requirements or could with minor modification such as increasing the available pressure [22].

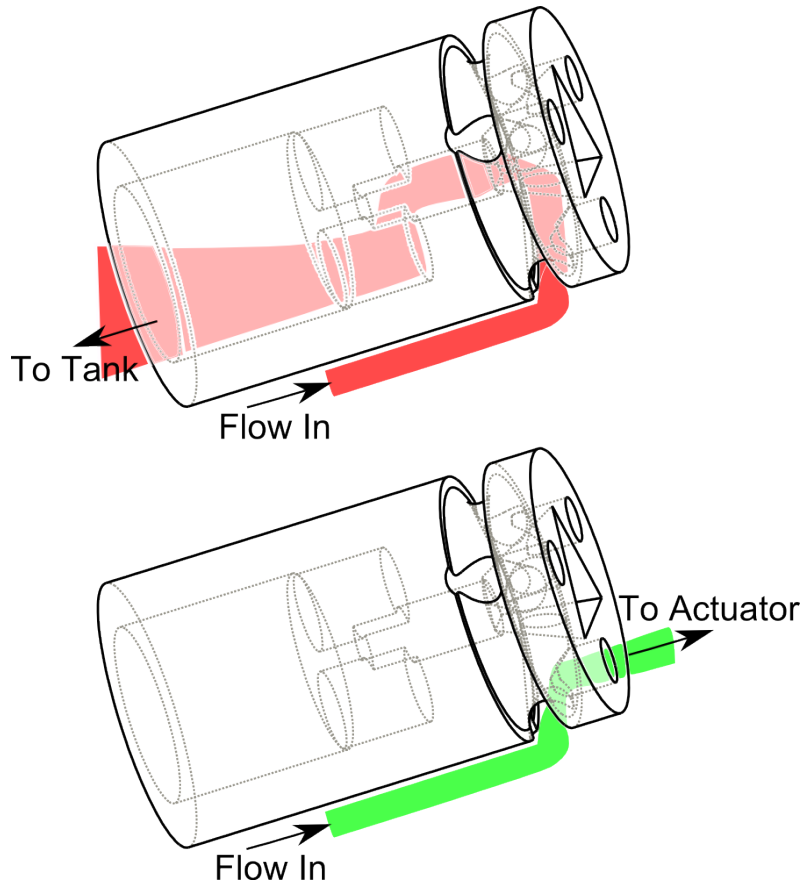


Figure 8.: Model of the control valve showing part of the flow path for both open (top) and blocked (bottom) variable orifice conditions.

## 6. Valve Prototyping and Experimental Results

### 6.1 Plug-Based Valve Testing

Both versions of the valve were also prototyped and tested. The plug-based version of the valve was printed using a Stratasys Dimension 1200es rapid prototyping machine at three times geometric scale such that the outer diameter was 18 mm. The orifices were scaled according to the flow characteristics (Section 3) such that the downstream orifice was 1.3 mm, upstream orifice was 0.74 mm, and the gap was 0.4 mm. A scaled prototype was selected due to difficulties associated with fabrication at the design scale (Fig. 13) for which the outer diameter is 6 mm, downstream orifice was 0.7 mm, upstream orifice was 0.4 mm, and gap was 0.25 mm. Shown in Fig. 14, one version of this valve prototype was made to be manually manipulated (Fig. 14a). To achieve this, a hole was drilled in the top cap of the valve to provide access to the inner plug. This hole is located downstream of the primary outlets at the same location as the intended return line such that the inclusion of this hole did not affect valve operation. A second prototype with a sealed cap was also produced (Fig. 14b). Included within this prototype was three electromagnetic coils intended to provide manipulative force to the inner plug. Each of these prototypes were fitted with a cylindrical ring to seal the outer supply channel and tubing to provide the necessary connections to the supply, return, and actuators. Each of these connections was rigidly sealed using steel reinforced epoxy (J-B Weld).

Pressure to the valves was supplied using a rotary vane pump (Procon) driven by an electric motor (Fig. 15). A relief valve was used to regulate the supply pressure at a steady 689 kPa. The flow rate from the pump was sufficient to provide constant pressure to the valves.

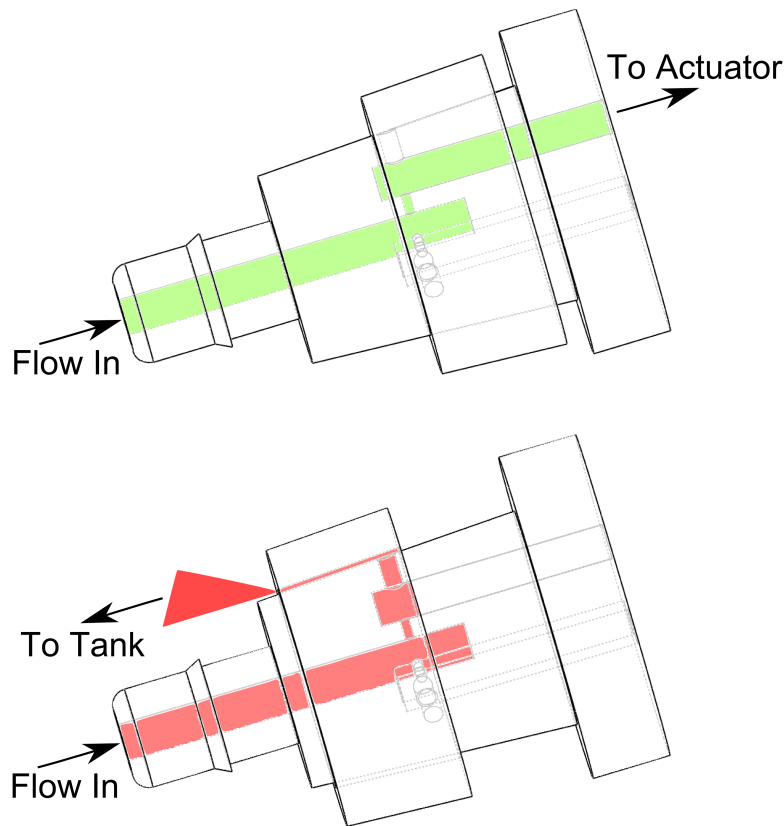


Figure 9.: Model of the ring-based control valve showing part of the flow path for both blocked (top) and open (bottom) variable orifice conditions.

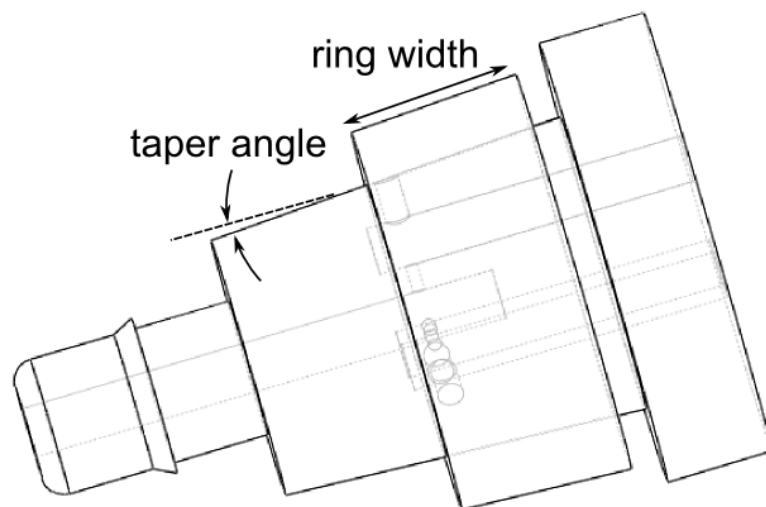


Figure 10.: Illustration of the ring-based valve showing the taper angle.

Manual manipulation of the valve plug demonstrated that it was possible to vary the pressure at the feed-points to each of the outlets that feed the actuators. However, the increase in pressure at the feed-point was not as large as was expected. Direct measurement of the pressure was not possible; however, estimations based on actuator inflation suggest a pressure of approximately 170 kPa, or 25% of the supply pressure, was achieved. From Fig. 3, it should be possible to achieve at least 90% of the supply pressure using the flapper valve. Possible causes for this may be poor geometric tolerances in the printing of the valve body or in the valve plug resulting in

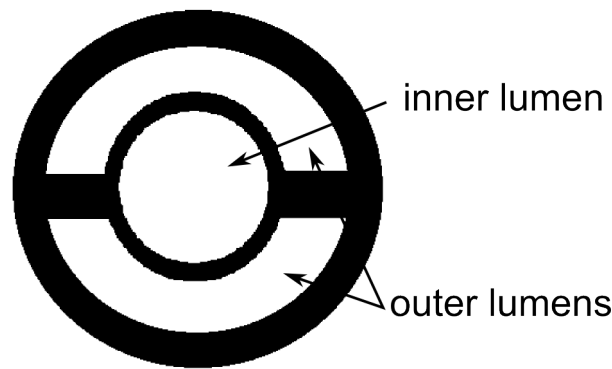


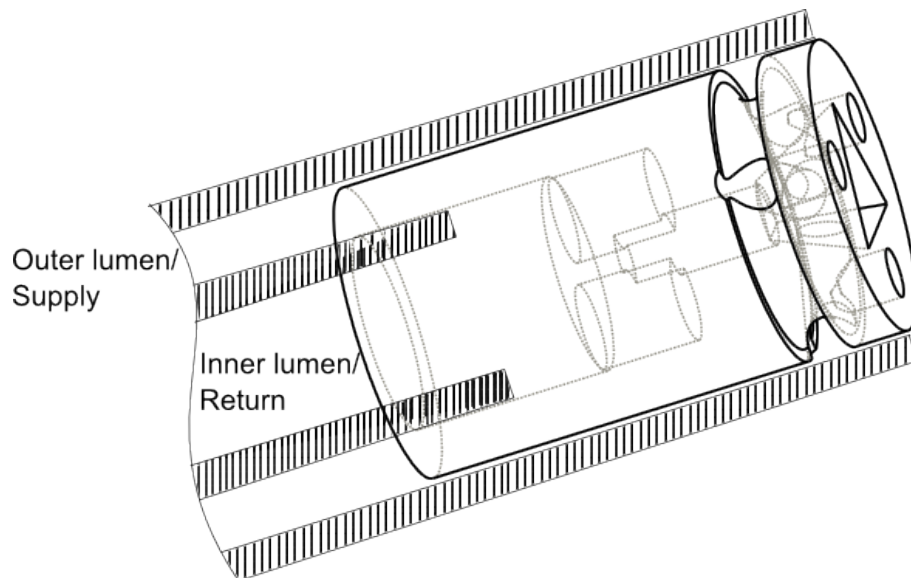
Figure 11.: Example cross-section of a multi-lumen tubing used to provide both feed and return lines for the control valve.

poor surface contact. In particular, the imprecision in the inside corners of the plug seat may have restricted the plug from closing the gap. Further, accessing the plug through the hole in the cap proved difficult and provided a limited range of motion. Using the electromagnetically manipulated valve in the same configuration produced similar results. A small change in feed-point pressure was observed but the change was not significant enough to produce any significant output at the actuator; an estimated pressure of 100 kPa or 15% of the supply pressure. This result may be due in part to higher flow forces at the valve orifice for the three times scale version of the valve. Increasing the diameter of the valve orifice significantly increases the flow forces at the valve plug. Further investigation is necessary to identify other possible sources of reduced pressure output.

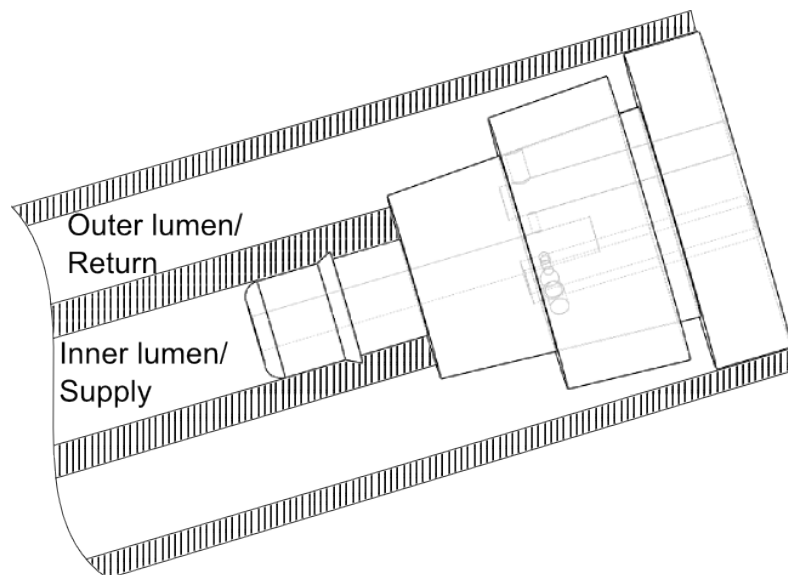
## 6.2 Ring-Based Valve Testing

The ring-based valve design was also prototyped and tested. However, to accommodate the need for manual manipulation and to reduce manufacturing costs, the scale of the valve was increased. At prototype scale, the outer dimension was 20 mm and the overall length was 32.5 mm. An upstream orifice diameter of 0.74 mm was used to provide the desired flow rate and then Eq. 5 resulted in a downstream orifice diameter of 1.3 mm in the fully open condition. Using this diameter, the necessary gap,  $g$ , between the orifice and the flapper under the fully open condition is 0.4 mm. Also, for this prototype, a taper angle of  $3^\circ$  was used in order to make manual manipulation of the valve ring possible. A prototype of this design is shown in Fig. 16. The prototype was produced using CNC machining techniques (Island Tool & Die, Pine Island, MN) and connected to the hydraulic lines using steel reinforced epoxy (J-B Weld) and a hose clamp, as shown in Fig. 17.

The ring-based valve prototype was tested using the same setup shown in Fig. 15. Testing of this prototype involved manual manipulation of the outer control ring to differentially open and close the flapper nozzles. It was found that the prototype of the ring-based design performed significantly better than the first design. It was possible to inflate artificial muscle actuators connected at the actuator feed points to their fully contracted states and thus the pressure increases at these locations were demonstrably superior than was observed for the first valve design, on the order of 650 kPa or 95% of the supply pressure. Further, it was possible to simultaneously increase the actuator outlet pressures in pairs by positioning the ring such that two orifices were sealed. Finally, it was found that the relative stiffness of the three outlets together could be manipulated by positioning the ring up or down the taper.



(a)



(b)

Figure 12.: Illustration of valve connection to the hydraulic supply and return lumens of the described tubing for the (a) plug-based valve design and (b) the ring-based valve design.

## 7. Summary of Control Valve Design

After review of the available valve technologies for control of a hydraulic system, no options were found at the scale necessary for this application. The design presented here is based on a single-jet flapper valve that facilitates control over the ratio of actuator pressure to supply pressure. The flapper valve design provides benefits of a relatively linear performance curve on the basis of outlet pressure versus downstream orifice size as shown in Fig. 3 [21]. The theoretical behavior of the valve is based on the principles of pressure drop across a flow restriction. As such, these predictions are dependent upon the quality and accuracy of the valve fabrication processes which can introduce unexpected errors due to poor surface finish or dimensional tolerances. For

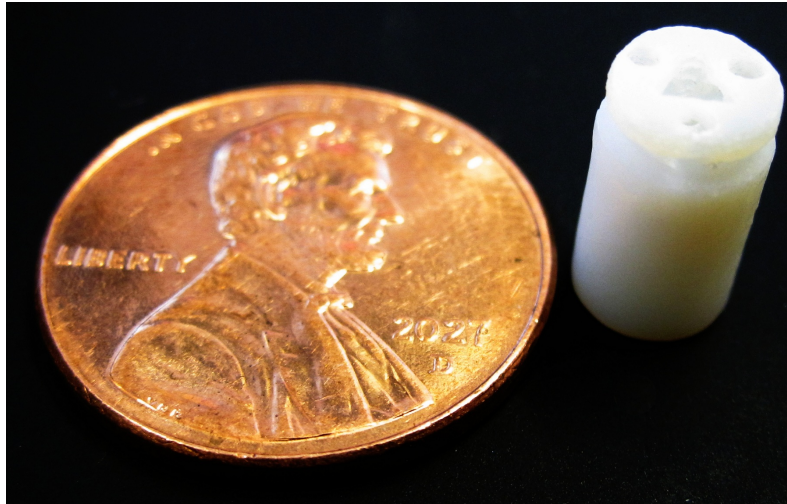
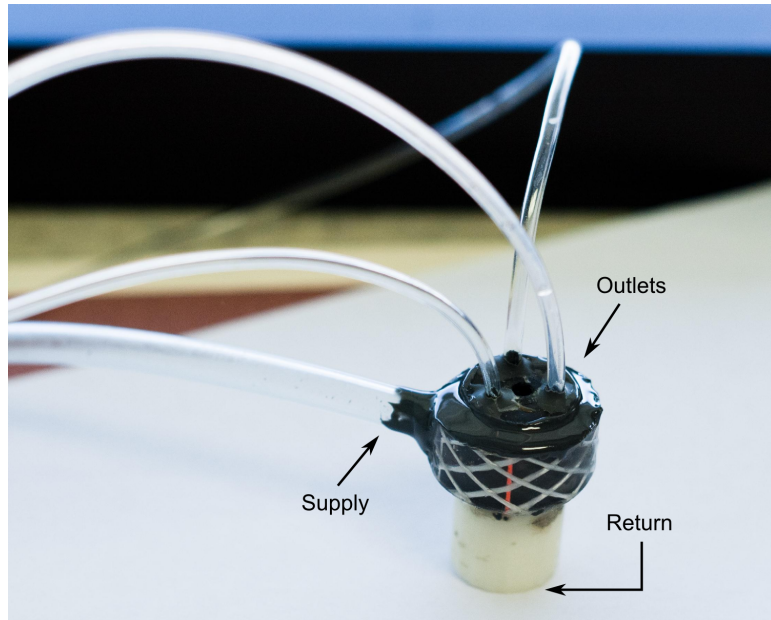


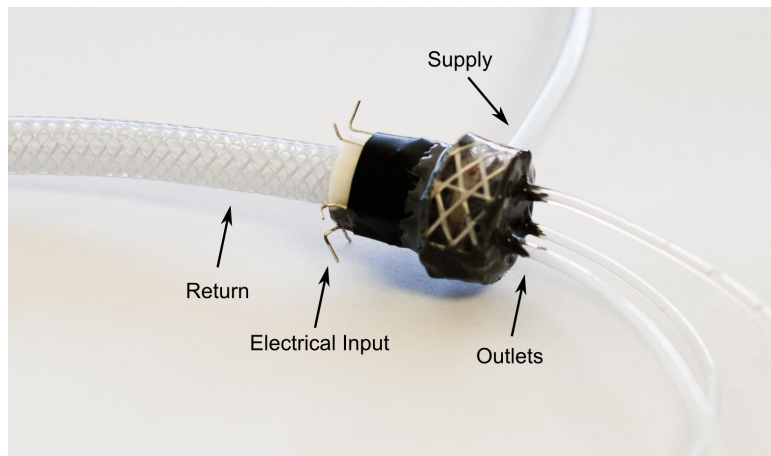
Figure 13.: Photograph of the design scale prototype of the plug-based valve design.

smaller valve orifices, these errors can become more pronounced. The valve design presented here consists of three such flapper nozzles for the control of three actuators. Two possible realizations of this design were discussed. Each realization contained a manipulated component (plug or ring) that plays the role of the flapper for each of the actuators, differentially opening and closing the three nozzles through planar motion. Further, axial motion of the plug or ring controls stiffness of the three actuators together.

Testing of the two prototyped valve realizations revealed that both were able to manipulate the pressure at the actuator feed points and further, the ring-based design performed significantly better than the plug-based design under similar operating conditions. It was possible to increase the pressure at the actuator feed points individually, in pairs, or all at the same time. These results indicate that this valve design represents a feasible solution for the control valve at design scale. Further, the valve design presented here provides a generalizable solution for the control of a multi-actuator robotic manipulator, particularly suited for manipulators operated in a differential and antagonistic fashion as is common for surgical manipulators designed for natural orifice surgery.



(a)



(b)

Figure 14.: Photographs showing the scaled plug-based valve prototype in both (a) manually manipulated and (b) electromagnetically manipulated configurations.

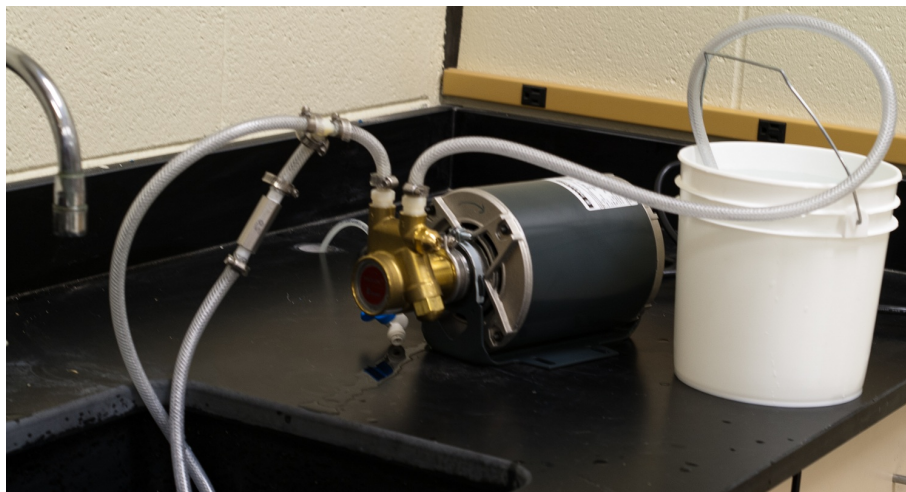
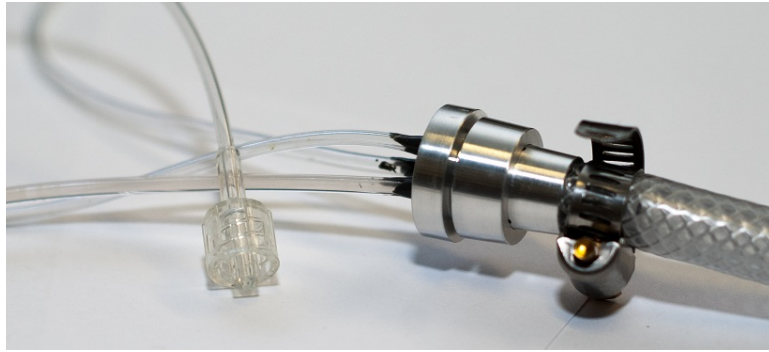


Figure 15.: Photograph of hydraulic supply setup.



Figure 16.: Machined prototype of the second valve design.



(a)



(b)

Figure 17.: Photographs showing the scaled valve prototype for the ring-based design with (a) outlet and supply lines attached and (b) assembled within the return line.

## References

- [1] Rattner D, Kalloo A. ASGE/SAGES working group on natural orifice transluminal endoscopic surgery. *Surgical Endoscopy*. 2006;20(2):329–333.
- [2] Love L, Lind R, Jansen J. Mesofluidic actuation for articulated finger and hand prosthetics. In: *Proceedings of the 2009 IEEE/RSJ international conference on intelligent robots and systems*. IEEE Press. 2009. p. 2586–2591.
- [3] Ho C, Tai Y. Micro-electro-mechanical-systems (MEMS) and fluid flows. *Annual Review of Fluid Mechanics*. 1998;30(1):579–612.
- [4] Whitesides G. The origins and the future of microfluidics. *Nature*. 2006;442(7101):368–373.
- [5] Berg DR. *Design of a Hydraulic Dexterous Manipulator for Minimally Invasive Surgery*. Phd. University of Minnesota. Minneapolis, MN. 2013 Sep. Available from: <https://doi.org/10.6084/m9.figshare.963287>.
- [6] Pourghodrat A, Nelson CA. Disposable fluidic actuators for miniature in-vivo surgical robotics. *Journal of Medical Devices*. 2017 Mar;11(1).
- [7] Pourghodrat A, Nelson CA, Oleynikov D. Hydraulic Robotic Surgical Tool Changing Manipulator. *Journal of Medical Devices*. 2017 Mar;11(1).
- [8] Linjama M, Vilenius M. Digital hydraulics - Towards perfect valve technology. In: *Proceedings of the tenth scandinavian international conference on fluid power*. Vol. 1. 2007. p. 181–196.
- [9] Studer V, Hang G, Pandolfi A, Ortiz M, Anderson W, Quake S. Scaling properties of a low-actuation pressure microfluidic valve. *Journal of Applied Physics*. 2004;95:393–398.
- [10] Luque A, Quero J, Hibert C, Flückiger P, Gañán-Calvo A. Integrable silicon microfluidic valve with pneumatic actuation. *Sensors and Actuators A: Physical*. 2005;118(1):144–151.
- [11] Baek J, Park J, Ju J, Lee T, Lee S. A pneumatically controllable flexible and polymeric microfluidic valve fabricated via in situ development. *Journal of Micromechanics and Microengineering*. 2005; 15:1015–1020.
- [12] Selvaganapathy P, Carlen E, Mastrangelo C. Electrothermally actuated inline microfluidic valve. *Sensors and Actuators A: Physical*. 2003;104(3):275–282.
- [13] Huff M, Mettner M, Lober T, Schmidt M. A pressure-balanced electrostatically-actuated microvalve. In: *IEEE Solid-State Sensor and Actuator Workshop, 4th Technical Digest*. 1990. p. 123–127.
- [14] Sounart T, Michalske T. Electrostatic actuation without electrolysis in microfluidic MEMS. In: *12th international conference on transducers, solid-state sensors, actuators and microsystems*. 2003. p. 615–618.
- [15] Ohnstein T, Fukiura T, Ridley J, Bonne U. Micromachined silicon microvalve. In: *Proceedings of ieee conference on micro electro mechanical systems*. 1990. p. 95–98.
- [16] Fikru N, Chase T. A review of MEMS based pneumatic valves. In: *2011 proceedings of the 52nd national conference on fluid power*. Las Vegas, NV: IEEE Press. 2011 Mar. p. 271–282.
- [17] Fu C, Rummler Z, Schomburg W. Magnetically driven micro ball valves fabricated by multilayer adhesive film bonding. *Journal of Micromechanics and Microengineering*. 2003;13(4):S96.
- [18] Pernod P, Preobrazhensky V, Merlen A, Ducloux O, Talbi A, Gimeno L, Viard R, Tiercelin N. MEMS magneto-mechanical microvalves (MMMS) for aerodynamic active flow control. *Journal of Magnetism and Magnetic Materials*. 2010;322(9):1642–1646.
- [19] Peirs J. Design of miniature parallel manipulators for integration in a self-propelling endoscope. *Sensors and Actuators A: Physical*. 2000;85(1-3):409–417.
- [20] Schulte H. The characteristics of the McKibben artificial muscle. In: *The application of external power in prosthetics and orthotics*. National Academy of Sciences National Research Council. 1961. p. 94–115.
- [21] Merritt H. *Hydraulic control systems*. John Wiley & Sons Inc. 1967.
- [22] Cheng L. *Development of an endoscopic irrigation pump: Experience with Byrne Medical, Inc.* [Ph.D. thesis]. Texas A&M University. 2007.
- [23] Oh KW, Ahn CH. A review of microvalves. *Journal of Micromechanics and Microengineering*. 2006 Mar;16(5):R13–R39. Available from: <http://doi.org/10.1088/0960-1317/16/5/R01>.
- [24] Richmond M. Solenoids and magnetic fields. nd. accessed: October 2011. Available from: [http://spiff.rit.edu/classes/phys313/lectures/sol/sol\\_f01\\_long.html](http://spiff.rit.edu/classes/phys313/lectures/sol/sol_f01_long.html).
- [25] Peikert R, Würtz D, Monagan M, de Groot C. Packing circles in a square: A review and new results. *System Modelling and Optimization*. 1992;:45–54.
- [26] Sloane N. Table of maximal density of a packing of equal spheres in n-dimensional euclidean

space (for  $n > 3$  the values are only conjectural). 2013. accessed: March 2013. Available from: <http://oeis.org/A093825/a093825.txt>.

[27] Incropera F, DeWitt D. Introduction to heat transfer. John Wiley and Sons Inc.. 1985.

[28] Sharqawy M, Lienhard J, Zubair S. Thermophysical properties of seawater: A review of existing correlations and data. Desalination and Water Treatment. 2010;16(1-3):354–380.

[29] Kreith F. The CRC handbook of thermal engineering. Springer. 2000.

[30] Ochkov V. Thermal conductivity of seawater and its concentrates. nd. accessed: June 2012. Available from: <http://twf.mpei.ac.ru/TTHB/2/Tab-5-5-13-2-Ther-Cond-Seawater.html>.

[31] Hewitt G. Heat exchanger design handbook. Begelle House Inc.. 1998.

[32] Berg DR. Plug valve design files. figshare. 2017 7;Available from: <https://doi.org/10.6084/m9.figshare.5248429.v1>.

[33] Berg DR. Ring valve design files. figshare. 2017 3;Available from: <https://doi.org/10.6084/m9.figshare.4765120.v1>.